

Original Article

Effect of Large Scale Electric Vehicle Loading on the Hopf Bifurcation Point in a Two Area System with and without Power System Stabilizer

Ghousul Azam Shaik¹, Lakshmi Devi Aithepalli²

^{1,2}Department of Electrical and Electronics Engineering, Sri Venkateswara University, Andhra Pradesh, India.

¹Corresponding Author : ghousul1993@gmail.com

Received: 15 November 2024

Revised: 17 December 2024

Accepted: 18 January 2025

Published: 25 January 2025

Abstract - This manuscript deals with the identification of the Hopf bifurcation point in a two-area system by the application of increased Electric vehicle load demand as a variable parameter. By considering a linearized static load model for electric vehicle load, a two-axis model for generator, and a quasi-steady state model for network expressed in power balance form, eigenvalue analysis was carried out with and without Power System Stabilizer (PSS). By taking eight cases and two scenarios in the Kundur two-area system, the sketching of the locus of inter-area mode was scripted in MATLAB 2020 environment to see the loading at which this value becomes purely imaginary. It can be inferred that the inclusion of PSS not only increased the damping of inter-area mode but also put off the Hopf bifurcation point till higher loading when compared to the base case of the first scenario. The eigenvalue analysis programme was repeated by taking a single line contingency as a second scenario, and the Hopf bifurcation point was sketched corresponding to the new base case and by accommodating newly tuned PSS, the efficacy of the same in putting off the dynamic stability limit till higher loading was proved by Hopf bifurcation analysis.

Keywords - Electric vehicle, Hopf bifurcation, Linearization, Load modelling, Small signal stability.

1. Introduction

The urge to promote green energy to reduce pollution for mobility has given birth to the usage of Electric Vehicles (EVs) in the conventional grid powered by various conventional and non-conventional energy sources. EVs can be used for both generation and as loads depending on the flexibility of customers. The large EV penetration into the grids will bring some challenges to the small signal stability, voltage instability and dynamic instability, which are addressed in this manuscript.

Representing various load models by Constant Power (CP), Constant Current (CI) and Constant Impedance (CZ) are very generic [1]. CP load representation for EV cannot be used if there is a severe voltage drop. Representing the EV load model as a polynomial combination of three models (ZIP) was proposed in [2]. To analyse the load flow of the distribution network in the presence of EVs, the ZIP load model was used by [2]. Only ensuring loss reduction and voltage improvement objectives aren't sufficient. The impact of these large EV load penetrations coupled to transmission systems powered by generators using detailed models is taken into account in this manuscript. Small signal stability is the ability of a system to remain stable under small disturbances. In order to study this, linearization of a generator coupled with an Automatic

Voltage Regulator (AVR), nominal 'pi' section transmission lines, non-linear voltage-dependent loads and other components needs to be done as stated in [3]. Applications of Power System Stabilizer (PSS) to improve the damping of electromechanical oscillations by using the worst damping ratio are found in [4]. The lower limit on the damping ratio is to be at least 3% under the worst conditions, as stated in [5]. Extensive reviews of different types of PSS design using time domain indices and damping ratios of eigenvalues in different types of systems are found in [6-8].

The usage of PSS in interconnected renewable systems can be found in [9]. If all eigenvalues of the overall system matrix obtained after linearization are within the left half of the s-plane, the system is small signal stable. Improving the damping ratio of critical eigenvalue can be done by optimizing PSS tuning. Tuning of PSS in an environment of a single generator source in a distributed system by taking the min-max fitness function using the PSO technique was studied by [10]. However, this paper only considered the worst damping ratio of all obtained eigenvalues to tune PSS.

Improving small signal stability in the Western States Coordinating Council (WSCC) under solar penetration by modelling loads as CP type is seen in [3]. The paper didn't



consider EV load modelling in multi-machine systems. Suppose one conjugate pair of eigenvalues traverses the imaginary axis while the remaining eigenvalues are still left in the left half of the s-plane boundary. In that case, this phenomenon is known as Hopf bifurcation. In order to accomplish this, either a single parameter or multiple parameters can be varied to see the non-linear system behaviour and check the birth of the limit cycles.

With the installation of a Static Var compensator to the WSCC system, the phenomena of Hopf bifurcation and corresponding P-V curves were studied [11]. Application of Hopf bifurcation concepts to Single Machine Infinite Bus (SMIB) system with Static Synchronous Series Compensators (SSSC) can be seen in the works of [12]. Conditions of critical stability using bifurcation analysis applied to interconnected DC microgrids with multiple droop control methodologies can be seen in the works of [13].

The usage of Hopf bifurcation concepts to a DC-DC converter feeding CP load, which is a pessimistic load known for its stability degradation, can be found in [14]. Identification of Hopf bifurcation point in the networked microgrid using the continuum method in the presence of EV is seen in [15]. Details of dynamics when these are coupled to a larger grid are missing in [15]. A new voltage stability transient mechanism analysis of the couple bifurcation theory with discrete wavelets in a 36-bus system was found in [16], which also uses SVC to avoid Hopf bifurcation.

The procedure for finding a bifurcation point in a system with both increased load and generation as variation parameters without PSS and with only AVR was discussed in our previous study. The procedure used a small power step to calculate equilibrium points for fixed system configuration in the WSCC system. In this manuscript, a variation of Hopf bifurcation due to system topology change in the Kundur two-area system is done.

Based on the literature gathered above, the following objectives were framed in Kundur two area system provided in Figure 1:

1. To analyse the effect of loading at the load buses represented by the EV load model on the dynamic instability with only AVR.
2. To evaluate the loci of inter-area mode by the placement of PSS and to project the importance of the same in putting off the bifurcation point beyond the value of critical loading obtained without PSS.
3. To sketch the loci of the inter-area mode with and without PSS by considering single tie line contingency after redesigning PSS for the new scenario.
4. To evaluate the damping ratios of each local swing mode of Kundur two area system from nominal loading till critical loading at Hof bifurcation point.

Eight cases were taken up in the above system, along with non-contingency and contingency of tie line scenarios, to provide in-depth insight into the concepts of Hopf bifurcation.

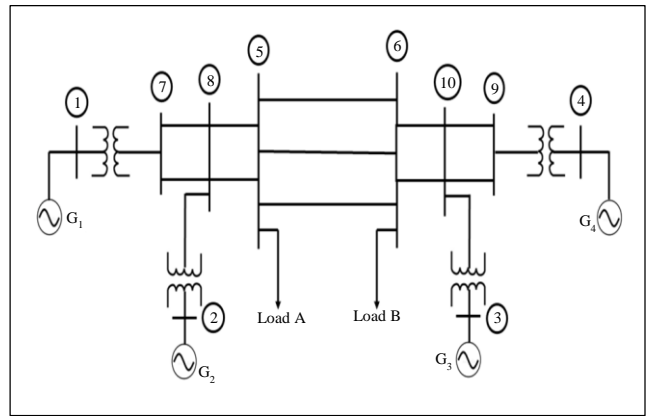


Fig. 1 Kundur two area system

2. Modelling of Power System Components & Concepts of Hopf Bifurcation

2.1. Modelling of Generator and Network

Two axis model was used to represent a synchronous machine whose details can be found in [17]. Static Exciter was represented by a first-order block of fixed time constant and gain. Transmission line was modelled by a medium pi circuit line followed by the application of power injection small signal models as given in [3] was used. For load flow sake, steady-state network parameters were obtained by taking load as CP type to obtain equilibrium points. PSS is used along with AVR as a remedial device for damping low-frequency electromechanical oscillations [3]. The first stage is a high pass filter of gain K_s and time constant T_Q . It is used to offset the controller in a steady state. The second stage comprises two lead-lag compensators of time constants T_1 , T_2 , T_3 , and T_4 , respectively, to provide sufficient phase lead when used in conjunction with the generator transmission network model, as shown in Figure 2. As damping of inter-area mode is necessary for multi-machine systems, T_Q is chosen as 10 s. The parameters of gain and other time constants are given in the simulation results section.

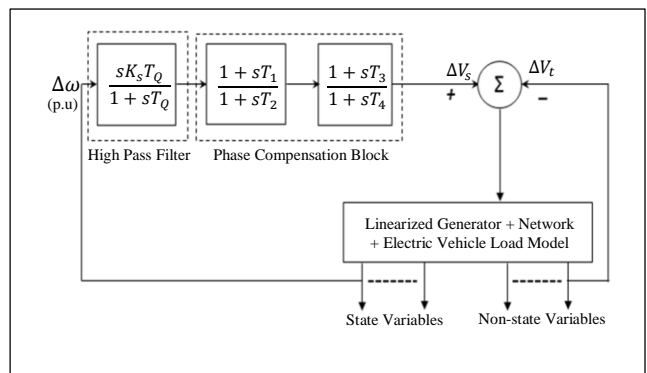


Fig. 2 Block diagram of PSS along with linearized power system model

2.2. Modelling of Static EV Load

Equations (1)-(4) and its associated nomenclature and parameters are borrowed from [2]. Parameters $\alpha_p, \beta_p, \gamma_p, \alpha_q, \beta_q, \gamma_q$ are -0.1773, 0.9949, 0.1824, 4.993, -12.910, 8.917 for EV static load model.

$$P = P_0 \left[\alpha_p + \beta_p \left(\frac{V}{V_0} \right) + \gamma_p \left(\frac{V}{V_0} \right)^2 \right] \quad (1)$$

$$Q = Q_0 \left[\alpha_q + \beta_q \left(\frac{V}{V_0} \right) + \gamma_q \left(\frac{V}{V_0} \right)^2 \right] \quad (2)$$

$$\alpha_p + \beta_p + \gamma_p = 1 \quad (3)$$

$$\alpha_q + \beta_q + \gamma_q = 1 \quad (4)$$

2.3. Mathematical Description of Hopf Bifurcation Phenomenon

The linearized system equations are represented by equations (5), (6). 'x', 'y', 'p' represent the state, algebraic and control variables, respectively.

$$x = f(x, y, p) \quad (5)$$

$$0 = g(x, y, p) \quad (6)$$

$$\nabla \dot{x} = \left[\frac{\partial f}{\partial x} \right]^0 \Delta x + \left[\frac{\partial f}{\partial y} \right]^0 \Delta y \quad (7)$$

$$0 = \left[\frac{\partial g}{\partial x} \right]^0 \Delta x + \left[\frac{\partial g}{\partial y} \right]^0 \Delta y \quad (8)$$

$$\nabla \dot{x} = [J_{SYS}] \Delta x \quad (9)$$

$$[J_{SYS}] = \left[\frac{\partial f}{\partial x} \right]^0 - \left[\frac{\partial f}{\partial y} \right]^0 \left[\left[\frac{\partial g}{\partial y} \right]^0 \right]^{-1} \left[\frac{\partial g}{\partial x} \right]^0 \quad (10)$$

$$P_{L,i} = P_{L,i,0} \lambda_i \quad (11)$$

$$Q_{L,i} = Q_{L,i,0} \lambda_i \quad (12)$$

Where $\lambda_i, P_{L,i,0}, Q_{L,i,0}$ represents loading factor, nominal real power and reactive power loading at i^{th} load bus, respectively.

Equations 5 and 6 are linearized using first-order Taylor series expansion about the steady state values of different non-state and state variables. Linearization of Equations 5 and 6 results in Equations 7 and 8. By proper matrix manipulation, Equations 9 and 10 are derived to assess stability. The linearization of the static EV load model is merged with linearized equations of the coupled network generator. The variation of parameter 'p' can follow either Equation 11 or both Equations 11 and 12 together. If all eigenvalues (J_{SYS})

given in Equation 10 lie in the left half of the s-plane, the system is small signal stable. Sometimes, for a given value of 'p', Equation (6) may not be solvable, which indicates that steady state values of network parameters don't exist for such type of loading. Even though Equation 6 is solvable for a given 'p', i.e. load flow Jacobian is non-singular, the eigenvalues (J_{SYS}) can cross the imaginary axis, and thus the dynamic instability is established. If only one conjugate pair of eigenvalues crosses the imaginary axis, such a phenomenon is known as Hopf bifurcation.

To observe whether the system undergoes Hopf bifurcation, parameter 'p' is varied and for each value of 'p', load flow is done to obtain network variables in steady-state. If one of the critical eigenvalues moves towards the imaginary axis, the value of 'p' at which this value crosses the imaginary axis is noted. Now, the investigation is repeated to see what value of the 'p' Hopf bifurcation point is extended with PSS device placement.

2.4. Application of Hopf Bifurcation Concepts to Sketch Loci of Critical Modes in Kundur Two Area System

- Step 1: Assume loads 'A' and 'B' as CP type for calculating steady-state network parameters using Newton Raphson method for each loading. Excess of load w.r.t base case loading at that load bus is compensated by increasing the generation of all generators corresponding to their inertia constants.
- Step 2: Use axis frame transformation to convert variables in the network frame of reference to a synchronous machine frame of reference. Calculate all the machine variables by moving the machine dynamic equations to zero [17].
- Step 3: Make incremental changes to all the ODEs of Machine, AVR, algebraic equations of stator, network algebraic equations using power injection model, static ZIP- EV load model, eliminate all non-state variables. Thus, the overall state matrix for each loading is obtained.
- Step 4: Ensure that all eigenvalues of the overall state matrix obtained in Step 3 lie in the left half of the s-plane. Identify "critical eigenvalue", which is the inter-area mode in this case. If yes, increase the loading parameter by a very small power step and repeat steps (1)-(3). If a pair of critical eigenvalues cross an imaginary line, stop. Note the load for which the bifurcation point is attained.
- Step 5: To accomplish the identification of the bifurcation point with PSS for scenario 1, place PSS at one of the generators and, by taking incremental changes to PSS dynamic equations, couple these with the ones obtained in step (3) to re-evaluate step (4) for finding Hopf bifurcation.
- Step 6: Remove one tie line between node numbers 5 and 6, which is defined as scenario 2. Recalculate load flow. Repeat the steps 1 to 5 once again. Redesign new PSS for scenario 2 and evaluate the EV loading effect on the Hopf bifurcation with and without PSS placement. For the

contingency of the tie-line scenario, it is assumed that the operator has sufficient time to disconnect the line. During this period, PSS gain and time constants can be modified, thus giving a glimpse into the concepts of dynamic tuning of PSS controller parameters.

The above-mentioned procedure is applied in Case A-H as defined below.

- Case A: Slow increase in the real power loading of the 5th bus without PSS.
- Case B: Slow increase in the real power loading of the 6th bus without PSS.
- Case C: Slow increase in both real and reactive power loading of the 5th bus without PSS.
- Case D: Slow increase in both real and reactive power loading of the 6th bus without PSS.
- Case E: Slow increase in the real power loading of the 5th bus with PSS.
- Case F: Slow increase in the real power loading of the 6th bus with PSS.
- Case G: Slow increase in both real and reactive power loading of the 5th bus with PSS.
- Case H: Slow increase in both real and reactive power loading of the 6th bus with PSS.

All the Cases A-H were executed in MATLAB environment by generating the following scenarios.

- Scenario 1: All three tie lines are in service, i.e. non-contingency of the tie lines.
- Scenario 2: A single-line contingency among three tie lines.

3. Simulation Results and Discussions

The Kundur two-area system has 4 generators, 10 nodes and 2 loads, as per Figure 1. G_4 is taken as a reference. System data is taken from [17, 18], except that the mechanical damping of all machines is taken as 0.01 p.u in this manuscript.

By taking the mechanical damping of machines as zero, the eigenvalues given in [18] were obtained exactly, proving the validation of code developed for constant impedance type of loading. The network is solved by using the Newton-Raphson method coded in MATLAB 2020 by representing the loads as constant power. For small signal stability studies, loads ‘A’ and ‘B’ are represented by static EV loads modelled by ZIP.

3.1. Discussions Regarding Scenario 1

Without PSS, the linearized model of the system is of the order 20, including the zero eigenvalue. This is because five state equations represent each machine model, and as there are four machines, the total number becomes 20. By not including

zero eigenvalues, the results of eigenvalue analysis without any PSS and with only AVR’s at all machines for no line contingency scenario 1 is tabulated in Table 1.

The damping ratios of swing modes ‘a’, ‘b’ and ‘c’ are 0.1043, 0.1095 and 0.0091, respectively. The first two rows of Table 1 represent the exciter modes. After placing PSS of the parameters $K_s= 17.2079$, $T_1= 0.2473$ s, $T_2= 0.0218$ s, $T_3= 3$ s, $T_4= 5.4$ s, $T_Q= 10$ s at G_4 , the damping ratio of swing modes changed to 0.1043, 0.3001, and 0.0508 respectively which shows significant improvement.

All the critical mode loci corresponding to scenario 1 are depicted in Figure 3. Hopf bifurcation is reached near the loading of 13.2 p.u. for Case A without PSS, as tabulated in Table 2. The damping ratio of swing modes ‘a’ and ‘b’ deteriorated to 0.0938 and 0.0951 from the base case damping ratio values projected in the above paragraph. The voltages at the 5th and 6th node for the above loading are 0.9699 p.u. and 0.9665 p.u. respectively.

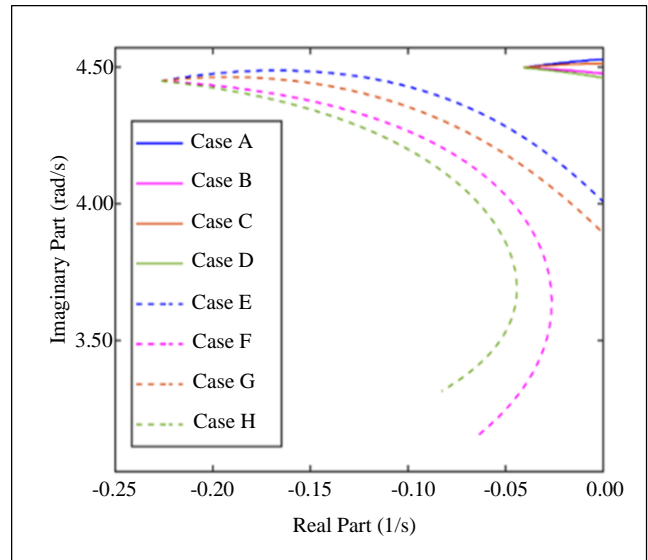


Fig. 3 Locus of critical eigenvalue to assess Hopf bifurcation for cases A-H corresponding to scenario 1

Hopf bifurcation is prolonged till the loading of 22.03 p.u. with PSS for Case E, which is more than the critical loading obtained for Case A as shown in Table 2 with the damping ratios of swing modes ‘a’ and ‘b’ decreased to 0.0437 and 0.1874. The values of voltages at nodes 5 and 6 are 0.8773 p.u. and 0.8660 p.u. respectively.

Hopf bifurcation is achieved near the loading of 17.24 p.u. for Case B without PSS as in Table 2, and at that loading, the damping ratios of swing modes ‘a’ and ‘b’ are 0.0942 and 0.0953 respectively. The voltages at the 5th and 6th nodes are 0.9671 p.u. and 0.9585 p.u. respectively. The Hopf bifurcation is not reached at a loading of 26.20 p.u. for Case F with PSS but for a loading of 26.22 p.u. load flow diverges.

Table 1. Eigenvalue analysis at nominal loading with and without PSS for two scenarios

Eigenvalues for Scenario 1		Eigenvalues for Scenario 2	
Without PSS	With PSS at G ₄	Without PSS	With PSS at G ₄
-24.7272 ± 20.3081i	-22.4313 ± 20.9601i	-24.7447 ± 20.3045i	-22.8772 ± 20.8957i
-25.1044 ± 11.4940i	-22.7956 ± 15.2786i	-25.0236 ± 13.7329i	-23.4654 ± 15.9845i
-0.7672 ± 7.3164i ^a	-0.7670 ± 7.3161i ^a	-0.7631 ± 7.2902i ^a	-0.7630 ± 7.2900i ^a
-0.7394 ± 6.7112i ^b	-1.9328 ± 6.1438i ^b	-0.7303 ± 6.6911i ^b	-1.8793 ± 6.3202i ^b
-0.0410 ± 4.4975i ^c	-0.2263 ± 4.4486i ^c	-0.0251 ± 3.9712i ^c	-0.1496 ± 3.9296i ^c
-39.5988, -40.0941	-39.9113, -57.1398	-39.4817, -39.8120	-39.6892, -55.9727
-11.5108, -11.1021	-14.2839, -11.2748	-11.6103, -11.3286	-14.1225, -11.4617
-4.0966, -4.2365	-4.0967, -4.2624	-4.1309, -4.2691	-4.1317, -4.2323
-4.4046, -4.5009	-4.4021, -4.4872	-4.4048, -4.5002	-4.4049, -4.5029
-0.0323	-0.0108, -31.9170	-0.0323	-0.0110, -31.1059
-	-0.1998 ± 0.1194i	-	-0.1983 ± 0.1182i

^a ((Swing mode associated with generators 1 and 2)); ^b ((Swing mode associated with generators 3 and 4)); ^c ((Inter-area mode))

Hopf bifurcation is reached at a loading factor λ_5 of 1.1545 for Case C without PSS, as given in Table 1, whose swing mode damping ratios are 0.0925 and 0.0934, respectively. The voltages at load buses 5 and 6 are 0.9626 p.u. and 0.9641 p.u. respectively. The critical loading factor λ_5 is extended till 1.8605 for Case G with PSS, which is greater than the value of the loading factor of Case C, thereby proving the efficacy of PSS device placement. The damping ratio of modes ‘a’ and ‘b’ are 0.0436 and 0.1869, respectively. The voltages at 5th and 6th nodes are 0.8326 p.u. and 0.8553 p.u. respectively.

Hopf bifurcation point is achieved at a loading of 1.0970 for Case D without PSS, which is lower than the loading of 1.5795 obtained for Case H with PSS placement, as is evident in Table 1. Voltage at nodes 5 and 6 are 0.9652 p.u. and 0.9521 p.u. respectively at the maximum loading corresponding to Case D. For a loading factor λ_6 of 1.5800, load flow doesn’t converge. Hence, eigenvalue analysis for a factor of 1.5795, as Case H, is shown in Table 1. Swing mode damping ratios ‘a’ and ‘b’ of Case D at the Hopf bifurcation point are given as 0.0939 and 0.0944, respectively.

3.2. Discussions Regarding Scenario 2

The results of eigenvalue analysis without any PSS and with only AVR’s at all machines for no line contingency by not including zero eigenvalues for scenario 2 are tabulated in Table 1. The damping ratios of swing modes ‘a’, ‘b’ and ‘c’ are 0.1041, 0.1085 and 0.0063, respectively. After placing the PSS of the parameters $K_s= 16.637$, $T_1= 0.2173$ s, $T_2= 0.0218$ s, $T_3= 3$ s, $T_4= 5.4$ s, $T_Q= 10$ s at G₄, the damping ratio of swing

modes changed to 0.1041, 0.2850, and 0.0380 respectively which shows significant improvement.

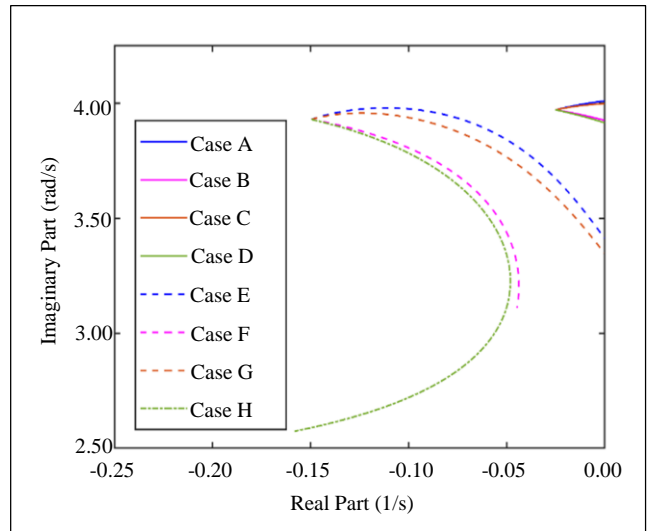


Fig. 4 Locus of critical eigenvalue to assess Hopf bifurcation for cases A-H corresponding to scenario 2

All the critical mode loci corresponding to scenario 2 are depicted in Figure 4. Hopf bifurcation is reached near the loading of 13.01 p.u. for Case A without PSS, as depicted in Table 3. The damping ratio of swing modes ‘a’ and ‘b’ deteriorated to 0.0948 and 0.0961 from the base case of scenario 2, whose damping ratios are obtained from Table 1. The voltages at the 5th and 6th node for the above loading are 0.9665 p.u. and 0.9622 p.u. respectively.

The Hopf bifurcation is prolonged till loading of 21.04 p.u. for Case E with PSS, which is more than critical loading obtained for Case A as shown in Table 3 with the damping ratios of swing mode ‘a’ and ‘b’ decreased to 0.0480 and 0.1836 respectively. The values of voltages at nodes 5 and 6 are 0.8790 p.u. and 0.8664 p.u. respectively at the maximum dynamic loadability limit for Case E.

Hopf bifurcation is achieved near the loading of 16.93 p.u. without PSS for Case B as in Table 3, and at that loading, the damping ratios of swing modes ‘a’ and ‘b’ are 0.0960 and 0.0968, respectively. The voltages at the 5th and 6th nodes are 0.9626 p.u. and 0.9532 p.u. respectively at the maximum loadability limit of Case B. Hopf Bifurcation is not reached at a loading of 22.85 p.u. for Case F with PSS but for a loading of 23.9 p.u. load flow diverges.

Hopf bifurcation is reached at a loading factor λ_5 of 1.1395 for Case C without PSS, as shown in Table 3, whose

swing mode damping ratios are 0.0933 and 0.0943, respectively. The values of load bus voltages at nodes 5 and 6 are 0.9595 p.u. and 0.9604 p.u. respectively. The critical loading factor λ_5 is extended till 1.7755 for Case G, which is greater than the value of the loading factor of Case C. It once again proved the efficacy of PSS device placement. The damping ratio of modes ‘a’ and ‘b’ are 0.0479 and 0.1849, respectively.

Hopf bifurcation point is achieved at a maximum loading of 1.0745 for Case D, which is lower than the critical loading of 1.4705 as obtained for Case H with PSS placement, as seen in Table 3. At the maximum loadability limit for Case D, the values of load bus voltages are 0.9617 p.u. and 0.9482 p.u. respectively. For a loading factor λ_6 of 1.4710, the load flow doesn’t converge. Hence, eigenvalue analysis for a factor of 1.4705 is shown in Table 3 for Case H. Swing mode damping ratio ‘a’ and ‘b’ of Case D at the Hopf bifurcation point is given as 0.0960 and 0.0963 respectively.

Table 2. Eigenvalue analysis at respective loadings for scenario 1 with and without PSS

Eigenvalues without PSS			
Case A (P₅=13.20 p.u.)	Case B (P₆=17.24 p.u.)	Case C ($\lambda_5 = 1.1545$)	Case D ($\lambda_6 = 1.0970$)
-24.6937 ±20.4624i	-24.7104 ±20.4859i	-24.7162 ±20.2990i	-24.7312 ±20.3449i
-25.1101 ±11.2991i	-25.1097 ±11.5713i	-25.1159 ±11.3583i	-25.1138 ±11.6294i
-0.6945 ± 7.3739i ^a	-0.6971 ± 7.3662i ^a	-0.6845 ± 7.3692i ^a	-0.6945 ± 7.3645i ^a
-0.6492 ± 6.7954i ^b	-0.6489 ± 6.7755i ^b	-0.6380 ± 6.8018i ^b	-0.6420 ± 6.7716i ^b
-0.0001 ± 4.5281i^c	-0.0002 ± 4.4754i^c	-0.0001 ± 4.5129i^c	-0.0001 ± 4.4603i^c
-40.1566, -39.6952	-40.0251, -39.5786	-40.0833, -39.6261	-39.9611, -39.5086
-11.4733, -11.0778	-11.5639, -11.1887	-11.5411, -11.1327	-11.6184, -11.2467
-4.6034, -4.5203	-4.6159, -4.4917	-4.6145, -4.5237	-4.6129, -4.4933
-4.3631, -4.1978, -0.0323	-4.3892, -4.2093, -0.0323	-4.3861, -4.2326, -0.0323	-4.4181, -4.2189, -0.0323
Eigenvalues with PSS at G₄			
Case E (P₅=22.03 p.u.)	Case F (P₆= 26.20 p.u.)	Case G ($\lambda_5 = 1.8605$)	Case H ($\lambda_6 = 1.5795$)
-21.8488 ±22.3567i	-19.9843 ±24.1576i	-21.5233 ±22.0437i	-19.9432 ±25.1407i
-23.1367 ±16.8081i	-24.6879 ±17.3801i	-23.6320 ±16.5095i	-24.7628 ±17.0502i
-0.3316 ± 7.5762i ^a	-0.2877 ± 7.5587i ^a	-0.3297 ± 7.5539i ^a	-0.3388 ± 7.5275i ^a
-1.2617 ± 6.6142i ^b	-0.9431 ± 6.7577i ^b	-1.2558 ± 6.6013i ^b	-0.9647 ± 6.7497i ^b
-0.0000 ± 4.0075i^c	-0.0652 ± 3.1466i^c	-0.0002 ± 3.8938i^c	-0.0828 ± 3.3147i^c
-57.5964, -39.1235	-57.8653, -38.2935	-57.5230, -38.6255	-57.8386, -38.4206
-16.1200, -12.1565	-17.4638, -12.8938	-16.3852, -12.5614	-18.0469, -12.7480
-5.1108, -4.7886	-5.1096, -4.8163	-5.1614, -4.8140	-5.0294, -4.7600
-5.1986 ± 0.2103i	-5.6305, -5.4275	-5.1980 ± 0.1988i	-5.6595, -5.3316
-0.2304 ± 0.1436i	-0.2436 ± 0.1528i	-0.2312 ± 0.1442i	-0.2623 ± 0.1610i
-30.2755, -0.0077	-29.4904, -0.0073	-29.9392, -0.0076	-28.7430, -0.0063

^{a)} ((Swing mode associated with generators 1 and 2)); ^{b)} ((Swing mode associated with generators 3 and 4)); ^{c)} ((Inter-area mode))

Table 3. Eigenvalue analysis at respective loadings for scenario 2 with and without PSS

Eigenvalues without PSS			
Case A ($P_5= 13.01$ p.u.)	Case B ($P_6= 16.93$ p.u.)	Case C ($\lambda_5= 1.1395$)	Case D ($\lambda_6= 1.0745$)
-24.7114 ±20.4320i	-24.7337 ±20.4365i	-24.7297 ±20.2871i	-24.7494 ±20.3233i
-25.0209 ±13.5633i	-25.0222 ±13.8795i	-25.0288 ±13.5653i	-25.0271 ±13.8868i
-0.6995 ±7.3445i ^a	-0.7070 ± 7.3294i ^a	-0.6883 ± 7.3422i ^a	-0.7065 ± 7.3278i ^a
-0.6534 ± 6.7679i ^b	-0.6558 ± 6.7437i ^b	-0.6416 ± 6.7765i ^b	-0.6518 ± 6.7398i ^b
-0.0001 ± 4.0096i^c	-0.0001 ± 3.9256i^c	-0.0001 ± 3.9980i^c	-0.0001 ±3.9151i^c
-11.5518, -11.2709	-11.6645, -11.4085	-11.6135, -11.3087	-11.7043, -11.4487
-39.5982, -39.9102	-39.4507, -39.7487	-39.5392, -39.8580	-39.3959, -39.7082
-4.2110, -4.3765	-4.2223, -4.3907	-4.2436, -4.3985	-4.2257, -4.4080
-4.5017, -4.5923, -0.0323	-4.4757, -4.5956, -0.0324	-4.5065, -4.6058, -0.0323	-4.4778, -4.5912, -0.0324
Eigenvalues with PSS at G₄			
Case E ($P_5= 21.04$ p.u.)	Case F ($P_6= 22.85$ p.u.)	Case G ($\lambda_5= 1.7755$)	Case H ($\lambda_6= 1.4705$)
-22.3813 ±21.9291i	-21.6494 ±22.5487i	-22.0833 ±21.6519i	-20.5380 ±24.8260i
-23.6137 ±17.9751i	-24.3512 ±17.5071i	-24.0424 ±17.4444i	-24.9960 ±18.5457i
-0.3620 ± 7.5368i ^a	-0.4309 ± 7.4768i ^a	-0.3606 ±7.5159i ^a	-0.3948 ± 7.4645i ^a
-1.2561 ± 6.7262i ^b	-1.2645 ± 6.6564i ^b	-1.2626 ± 6.7111i ^b	-0.9912 ± 6.7894i ^b
-0.0001 ± 3.4129i^c	-0.0447 ± 3.1094i^c	-0.0003 ± 3.3490i^c	-0.1582 ±2.5744i^c
-0.2310 ± 0.1446i	-0.2160 ± 0.1347i	-0.2301 ± 0.1440i	-0.2082 ± 0.1299i
-56.3547, -39.0389	-56.3240, -38.8576	-56.3125, -38.5948	-56.4750, -38.3017
-15.6234, -12.2154	-15.7998, -12.3238	-15.7126, -12.5755	-17.2117, -12.8264
-5.0802, -4.7395	-4.7983, -4.6735	-5.1167, -4.7633	-4.9665, -4.6586
-5.1389 ± 0.2031i	-5.1388 ± 0.0506i	-5.1263 ± 0.1917i	-5.6112, -5.2264
-29.9777, -0.0076	-29.9545, -0.0093	-29.8672, -0.0077	-29.2360, -0.0105

^{a)} ((Swing mode associated with generators 1 and 2)); ^{b)} ((Swing mode associated with generators 3 and 4)); ^{c)} ((Inter-area mode))

4. Conclusion and Future Work

The Hopf bifurcation method was explored on the Kundur two-area system without any PSS by keeping large-scale EV load as a variable parameter to sketch the locus of critical inter-area mode. With the placement of properly tuned PSS, it was proved that the critical loading could be extended far beyond the base case without PSS placement for both non-contingency and contingency of tie-line scenarios, thus addressing variation of critical loading at the load bus with the structural changes of the transmission network as well. The

degradation of damping ratios of local swing modes of each area at the critical loading, both with and without PSS, for both scenarios were also presented. In future, renewable sources integrated with EV load interaction with PSS in the grid can be studied.

Funding Statement

Ghousul Azam Shaik thanks the University Grants Commission (UGC), New Delhi, India, for providing a Junior Research Fellowship during the PhD program.

References

- [1] C. Concordia, and S. Ihara, "Load Representation in Power Systems Stability Studies," *IEEE Transactions on Power Apparatus and Systems*, vol. PAS-101, no. 4, pp. 969-977, 1982. [[CrossRef](#)] [[Google Scholar](#)] [[Publisher Link](#)]
- [2] Bables K. Jha et al., "A Modified Current Injection Load Flow Method under Different Load Model of EV for Distribution System," *International Transactions on Electrical Energy Systems*, vol. 30, no. 4, 2020. [[CrossRef](#)] [[Google Scholar](#)] [[Publisher Link](#)]
- [3] Prasenjit Dey et al., "Analysis of the Effects of PSS and Renewable Integration to an Inter-Area Power Network to Improve Small Signal Stability," *Journal of Electrical Engineering & Technology*, vol. 15, no. 5, pp. 2057-2077, 2020. [[CrossRef](#)] [[Google Scholar](#)] [[Publisher Link](#)]

- [4] Md. Rashidul Islam et al., "Power System Stability Enhancement through Optimal PSS Design," *e-Prime - Advances in Electrical Engineering, Electronics and Energy*, vol. 9, 2024. [[CrossRef](#)] [[Google Scholar](#)] [[Publisher Link](#)]
- [5] Xi-Fan Wang, Yonghua Song, and Malcolm Irving, *Modern Power Systems Analysis*, Springer, New York, 2008. [[CrossRef](#)] [[Google Scholar](#)] [[Publisher Link](#)]
- [6] J. Renedo, L. Sigríst, and L. Rouco, "Design of Power System Stabilizers to Damp Low Frequency Inter-Area Oscillations with Limited Information," *2019 IEEE Milan PowerTech*, Milan, Italy, pp. 1-6, 2019. [[CrossRef](#)] [[Google Scholar](#)] [[Publisher Link](#)]
- [7] Ramesh Devarapalli, Nikhil Kumar Sinha, and Fausto Pedro García Márquez, "A Review on the Computational Methods of Power System Stabilizer for Damping Power Network Oscillations," *Archives of Computational Methods in Engineering*, vol. 29, no. 6, pp. 3713-3739, 2022. [[CrossRef](#)] [[Google Scholar](#)] [[Publisher Link](#)]
- [8] Adrian Nocoń, and Stefan Paszek, "A Comprehensive Review of Power System Stabilizers," *Energies*, vol. 16, no. 4, 2023. [[CrossRef](#)] [[Google Scholar](#)] [[Publisher Link](#)]
- [9] Mohamad Almas Prakasa et al., "A Hybrid Controlling Parameters of Power System Stabilizer and Virtual Inertia Using Harris Hawk Optimizer in Interconnected Renewable Power Systems," *IEEE Access*, vol. 12, pp. 76219-76243, 2024. [[CrossRef](#)] [[Google Scholar](#)] [[Publisher Link](#)]
- [10] Kulsomsup Yenchanalit et al., "Control of Low-Frequency Oscillation on Electrical Power System under Large EV-Charging Station Installation Using PSO Technique for Turning PSS Parameters," *International Review of Electrical Engineering*, vol. 16, no. 5, pp. 401-408, 2021. [[CrossRef](#)] [[Google Scholar](#)] [[Publisher Link](#)]
- [11] Mark J. Laufenberg, M.A. Pai, and K.R. Padiyar, "Hopf Bifurcation Control in Power Systems with Static Var Compensators," *International Journal of Electrical Power & Energy Systems*, vol. 19, no. 5, pp. 339-347, 1997. [[CrossRef](#)] [[Google Scholar](#)] [[Publisher Link](#)]
- [12] R.C. Mala, Nagesh Prabhu, and H.V. Gururaja Rao, "Hopf Bifurcations of Subsynchronous Resonance in a Hybrid Series Compensated System with SSSC-ES," *2015 International Conference on Technological Advancements in Power and Energy (TAP Energy)*, Kollam, India, pp. 65-72, 2015. [[CrossRef](#)] [[Google Scholar](#)] [[Publisher Link](#)]
- [13] Haiyuan Liu et al., "Stability and Bifurcation Analysis of DC Microgrid with Multiple Droop Control Sources and Loads," *IEEE Transactions on Power Electronics*, vol. 36, no. 2, pp. 2361-2372, 2021. [[CrossRef](#)] [[Google Scholar](#)] [[Publisher Link](#)]
- [14] Liangyu Huang, and Yimin Lu, "Discrete Modeling and Period-Adding Bifurcation of DC-DC Converter Feding Constant Power Load," *IEEE Access*, vol. 9, pp. 52773-52783, 2021. [[CrossRef](#)] [[Google Scholar](#)] [[Publisher Link](#)]
- [15] Xinyuan Jiang et al., "Identifying Hopf Bifurcations of Networked Microgrids Induced by the Integration of EV Charging Stations," *2021 IEEE Transportation Electrification Conference & Expo (ITEC)*, Chicago, IL, USA, pp. 690-694, 2021. [[CrossRef](#)] [[Google Scholar](#)] [[Publisher Link](#)]
- [16] Yawei Wei et al., "Renewable Integrated Transient Voltage Stability Mechanism Analysis Using Hopf Bifurcation and Discrete Wavelet Transform," *2021 International Conference on Power System Technology (POWERCON)*, Haikou, China, pp. 1737-1742, 2021. [[CrossRef](#)] [[Google Scholar](#)] [[Publisher Link](#)]
- [17] Peter W. Sauer, M.A. Pai, and Joe H. Chow, *Power System Dynamics and Stability: With Synchrophasor Measurement and Power System Toolbox*, 2nd Ed., Wiley-IEEE Press, 1998. [[Google Scholar](#)] [[Publisher Link](#)]
- [18] M.A. Pai et al., *Small Signal Analysis of Power Systems*, Narosa Publishing House, New Delhi, 2004. [[Google Scholar](#)] [[Publisher Link](#)]